Diblock Copolymer Melt in Spherical Unit Cells of Higher Dimensionalities

M. Banaszak*, A. Koper, P. Knychała and K. Lewandowski
Faculty of Physics, A. Mickiewicz University, Umultowska 85, 61-614 Poznań, Poland

(Received April 27, 2011)

Using self-consistent field theory in spherical unit cells of various dimensionality, $D = 1$, 2, 3, and 4, we calculate phase diagram of a diblock, A-b-B, copolymer melt in 4-dimensional space, $d = 4$. The phase diagram is parameterized by the chain composition, f, and incompatibility between A and B, quantified by the product χN. We predict 4 stable nanophases: layers, cylinders, $3D$ spherical cells, and $4D$ spherical cells. We also calculate order–disorder and order–order transition lines. In the strong segregation limit, that is for large χN, the order–order transition compositions are determined by the strong segregation theory in its simplest form, for $D = 1$, 2, 3, and 4.

PACS: 82.35.Jk

1. Introduction

It is known that dimension, d, of a polymer system can play a significant and illuminating role. For example, single polymer chain in good solvent has the scaling properties of the self-avoiding walk (SAW) with the squared end-to-end distance varying as $\mathcal{R}^2 \sim N^{2\nu}$, where $\nu \approx 0.588$ for large N (often approximated as 0.6) for $d = 3$ [1], and N is the degree of polymerization (number of segments). This is a strongly fluctuating system which cannot be treated successfully by the mean-field (MF) approach. However, as d is increased to 4, and higher dimensions, the excluded volume interactions become a relatively small perturbation and the exponent ν becomes $1/2$ which is characteristic for free random walks (not self-avoiding) and free diffusion. Following Flory's idea it can be shown [1], in a simple analysis, that

$$\nu = \frac{3}{d+2}, \tag{1}$$

which works remarkably well for $d = 1$, 2, 3, and 4 yielding 1, $3/4$, $3/5$, and $1/2$, respectively. For a single chain the excluded volume interaction are suppressed for higher d, but the system still strongly fluctuates with $\nu = 1/2$.

In dense polymer system d can also play an important role, although both excluded volume interactions and fluctuations are suppressed for most of thermodynamic states. The suppression (screening) of excluded volume interactions, resulting in scaling exponent $\nu = 1/2$, is known as Flory's theorem and is well established for $d = 3$ [1]. The fluctuations are small, unlike in simple fluids in $3d$, because the environment is uniform and the coordination number, varying as $\sqrt{N}$, is large for long polymer chains [2]. While MF works remarkably well for most conditions, there are some exceptions, for example the composition fluctuations for homopolymer blends (vicinity of the macrophase separation) and for copolymer melts (near the order–disorder transition).

Diblock copolymer (DBC), A-b-B, melts can self-assemble in $3d$ into various spatially-ordered nanophases, such as layers, L, hexagonally packed cylinders, C, gyroid nanostructures, G, with the $Ia\bar{3}d$ symmetry, and cubically packed (either body-centered or closely packed) spherical cells S, depending on the chain composition, f (f is the fraction of A-segments; $1 - f$ is the fraction of B-segments), degree of polymerization (number of segments), N, and the temperature-related χ parameter [2, 3]. Recently, an additional O^{70}-phase has been reported [4, 5], but it is stable in a very small region of the phase diagram. Those nanophases can be transformed into a disordered phase, for example, upon heating. It is of great interest to determine a phase diagram of such melts exhibiting order–disorder transition (ODT) lines, also referred to as binodals of microphase separation transition (MST), and order–order transition (OOT) lines. This task has been largely achieved for 3-dimensional (bulk) diblock melts by accumulating results from numerous experimental and theoretical studies [6–13], also for $2d$ diblock copolymer melts [14].

The L, C, and S nanophases are known as classical, whereas G and O^{70} cubic nanophases are referred to as non-classical, or sometimes complex. The Wigner–Seitz cell of a classical phase can be approximated by D-dimensional sphere, S_D, both in the real $\boldsymbol{r}$-space and the reciprocal $\boldsymbol{k}$-space.

Within this approximation, known as unit cell approximation (UCA), the L, C, S nanophases correspond to S_1, S_2, and S_3, respectively, and the spacial distribution of chain segments can be mapped with a single radial variable, r, as shown in Table I. The classical phases can be easily generalized to higher dimensions, in particular for $d = 4$ we have 4 nanophases S_D, with dimensionality, D, ranging from 1 to 4. For $d = 3$ the non-classical phases are known to be stable in the vicinity of the ODT lines. Whether they are stable away from the ODT, in the strong segregation regime, is not entirely clear. There is some evidence that the G phase can exist up to a very strong segregation [15, 16], but it is not conclusive since it is based on MF calculations. Therefore one

* corresponding author; e-mail: mbanasz@amu.edu.pl

can conjecture that the stability of non-classical phases is enhanced by fluctuations (which are significant in the vicinity of the ODT), and the non-classical phases may not survive at very high values of χN. We also expect that the strength of fluctuations should diminish with increasing d. If the above conjecture is correct, then we should expect that, as the fluctuations grow weaker with increasing d, the non-classical phases should be less stable, or perhaps totally unstable for large d's. Could it be that the fluctuations can create the relative richness of non-classical nanophases for $d = 3$ and fewer complex phases for higher d's?

TABLE I

Unit cell equations of D-dimensionality; equations are supplemented with the unconstrained variables for corresponding d's (2, 3, 4 and 5); * indicates the absence of unconstrained variables; imp indicates that the nanophase for this d is impossible.

D	Nanophase	Cell equation	$d=2$	$d=3$	$d=4$	$d=5$	Radial coordinate
1	L (S_1)	$x^2 < R^2$	y	y, z	y, z, t	y, z, t, v	$r = \lvert x \rvert$
2	C (S_2)	$x^2 + y^2 < R^2$	*	z	z, t	z, t, v	$r = \sqrt{x^2 + y^2}$
3	S_3	$x^2 + y^2 + z^2 < R^2$	imp	*	t	t, v	$r = \sqrt{x^2 + y^2 + z^2}$
4	S_4	$x^2 + y^2 + z^2 + t^2 < R^2$	imp	imp	*	v	$r = \sqrt{x^2 + y^2 + z^2 + t^2}$
5	S_5	$x^2 + y^2 + z^2 + t^2 + v^2 < R^2$	imp	imp	imp	*	$r = \sqrt{x^2 + y^2 + z^2 + t^2 + v^2}$

Before we consider the $d = 4$ case, it may be useful to confront the $d = 2$ and $d = 3$ cases. For $d = 2$ the S_1 and S_2 nanophases are observed, and the non-classical phases cannot be formed, probably due to topological constraints, in this dimension. For $d = 3$, as already mentioned, the S_1, S_2, S_3 and non-classical nanophases are observed. The Wigner–Seitz cells for non-classical phases are not easily approximated by S_D's. The intricate spacial structures of non-classical nanophases is formed as a result of delicate competition between stretching energy (which is of entropic origin) with the interfacial energy (of enthalpic origin). The sequence of classical phase upon varying f from $1/2$ to 1 follows the order of increasing dimensionalities, D, which means that as f increased the S_D-phases with higher D's are observed.

Therefore, it might be interesting and relevant to investigate the higher-d phase behavior of copolymer melts. In this study, we do not limit d to 1, 2, and 3, but consider formally an arbitrary d, and $d = 4$ in particular. Thus, in addition to S_1, S_2, and S_3 nanophases, we consider the S_4 nanophase, and its thermodynamic stability.

It is interesting that a MF theory applied to copolymer melts [9, 17, 18], known as the self-consistent field theory (SCFT), is successful in predicting diblock phase diagrams resembling the experimental ones, as shown, for example, in Ref. [19]. The SCFT approach is based on the assumption that coarse-grained polymer chains in dense melts are Gaussian (already mentioned as Flory's theorem [1]), and on the MF approximation which selects the dominant contribution in the appropriate partition function, thus neglecting fluctuations. The SCFT can be applied to a variety of diblock copolymer phenomena, for example Cheng et al. [20] have studied the nucleation of ordered phases and the minimum energy paths. Moreover, the diblock copolymers in selective solvent [21, 22] and diblock semiflexible copolymers [23] have also been studied recently via SCFT. Another important SCFT work focuses on diblock copolymers with amphiphilic segments [24] and the cooperative assembly of mixtures of two types of diblocks [25].

It may be worth to reiterate that, despite a considerable success of the SCFT, the fluctuations can also play a significant role in determining the phase diagram of DBC melt for $d = 3$. For example, Fredrickson and Helfand [26] showed that Leibler's phase diagram [6] (based on 4th order MF free energy expansion into small composition variations in the Fourier space) can be considerably modified by the one-loop approximation of Brazovskii [27]. Similarly Fredrickson and co-workers show, in field simulations [12], that inclusion of fluctuations significantly improves the overall agreement of theory with experiment. In particular, those simulations [12] show a direct transition from disordered phase to C and G nanophases like in experiment [19] and particle Monte Carlo simulation [28, 29], but unlike the SCFT phase diagram [9].

Because, in the MF theories, it is sufficient to know the composition, f, and the product χN in order to foresee the nanophase [6, 18, 30], the diblock phase diagram can be mapped in (χN, f)-plane. The MF theories exist in many variations, both in real space ($\boldsymbol{r}$-space) [7, 8, 10] and the Fourier space ($\boldsymbol{k}$-space) [2, 9]. While $\boldsymbol{k}$-versions of the SCFT are more successful in predicting DBC phase diagram (in particular, the stability of the non-classical G phase [9, 18]) we limit the scope of this work to an $\boldsymbol{r}$-version, based on the UCA method. In this approach, the Wigner–Seitz cell of a periodic nanophase is approximated by a S_D-sphere. Effectively, a single radial variable, r, is used, as shown in Table I. Let us note that d is the dimension of the space, and D is the dimensionality of the spherical cell. Since a nanophase can have unconstrained spatial variables (for example, variable z for cylinders in $d = 3$), as indicated in Table I, D can

be smaller than d. As seen from this table, the non-classical phases are not considered in this method. The UCA method does not determine the spatial arrangement of the S_D spheres. For example, we do not know, from this theory, that the S_2-spheres (of the C phase) are hexagonally packed. Similarly, we do not know the spatial arrangement of the S_4-spheres. In order to find the equilibrium phase, different D's and radii, R, of spherical cell, are probed in the (χN, f)-parameter space. For very large χN's, the r-version of UCA tends to fail (for $\chi N > 130$), and therefore it is significant that Matsen developed a modified UCA method [11] using the Fourier–Bessel decomposition of radial functions. This improved method works, at least for χN's up to 1400, but since we limit the scope to $\chi N \leq 130$, it is sufficient to use the standard r-version of the SCFT for the main goal of this work. It is worthwhile to notice that in a recent study Matsen [31], using the spectral method with Anderson mixing, was able to perform the SCFT calculations up to $\chi N = 512000$.

In addition, we intend to compare the phase boundaries calculated by the SCFT (and extrapolated to the strong segregation limit, SSL) with the strong segregation theory (SST) for diblock melts, developed by Semenov [32], in which the free energy of the nanophase has three contributions, the interfacial tension and the stretching energies of the A and B blocks. These energies can be approximated by simple expressions, allowing the calculation of the OOT compositions in the SSL. Matsen and Whitmore [10] compared the extrapolations of the SCFT in the strong segregation limit with the SST results, obtaining a reasonable agreement, but with some discrepancy for the OOT compositions. The SST was modified by Likhtman and Semenov to include appropriate corrections [33]. In the zeroth order, the modified SST is equivalent to the original SST, but the leading correction suggests that the SCFT extrapolation should employ a different form of χN dependence in extrapolations, that is $(\chi N)^{-1/3}$ rather than $(\chi N)^{-1}$ used in Ref. [10]. However, the higher order corrections to the SST may also be important, and this may require another extrapolation dependence for χN in the SSL. Recently, Matsen [31] showed that $(\chi N)^{-1/3}$ scaling can, indeed, be observed for very high values of $\chi N = 512000$ which are beyond the scope (and capability) of this study. To summarize, we use the zeroth order of the SSL, and the $(\chi N)^{-1}$ scaling, for the following reasons:

- it is the simplest approach, and the exact scaling is not known,
- the first order correction, leading to the $(\chi N)^{-1/3}$ scaling, is observed for much higher values of χN than those used in this study,
- the agreement between the extrapolated SCTF and the SST is not crucial for the main result of this paper,
- the asymptotic agreement of SST and SCFT is very important for consistency reasons, but from the practical point of view, the high values of χN's, used in testing this consistency, seem to be beyond the physical reach.

The main goal of this paper is to construct a phase diagram of a copolymer melt in $4d$ applying the SCFT method with the UCA in r-space, as presented in [7–9]. Specifically, we intend to determine the area in (χN, f)-space, in which the S_4 phase is stable, by varying both the radius, R, of the unit cell and the dimensionality, D.

In this work, the following questions are posed:

1. is the S_4 nanophase stable?
2. what is the sequence of nanophases, upon changing f?
3. are the binodals (ODT lines) shifted as we vary d from 2 to 3, and from 3 to 4?
4. what are the strong segregation limits of the OOT lines, and are those limits close to the predictions of the strong segregation theory?

Beyond the scope of this study is the question concerning the stability of non-classical phases for higher d's. However if, indeed, the formation of the non-classical phases is enhanced by fluctuations (which are smaller for higher d's), then the MF results may be more relevant and accurate as we increase d to 4 and higher.

2. Method

The incompressible copolymer melt is modeled as a collection of n diblock chains confined in volume V. Each chain, labeled $\alpha = 1, 2, \ldots, n$, can take any Gaussian configuration (in accordance with the Flory's theorem [1]) parameterized from $s = 0$ to $s = f$ for A-segments, and from $s = f$ to $s = 1$ for B-segments. Up to a multiplicative constant, the partition function for a *single* Gaussian chain in external fields $W_A(\boldsymbol{r})$ and $W_B(\boldsymbol{r})$ acting on segments A and B, respectively, is

$$\mathcal{Q}[W_A, W_B] \equiv \int \tilde{\mathcal{D}}\boldsymbol{r}_\alpha(\cdot) \exp\left(- \int_0^f \mathrm{d}s W_A(\boldsymbol{r}_\alpha(s)) - \int_f^1 \mathrm{d}s W_B(\boldsymbol{r}_\alpha(s))\right). \quad (2)$$

The path integral, $\int \tilde{\mathcal{D}}\boldsymbol{r}_\alpha(\cdot)$, is taken over single-chain trajectories, $\boldsymbol{r}_\alpha(s)$, with the Wiener measure expressed as $\tilde{\mathcal{D}}\boldsymbol{r}_\alpha = \mathcal{D}\boldsymbol{r}_\alpha P[\boldsymbol{r}_\alpha; 0, 1]$, and

$$P[\boldsymbol{r}_\alpha; s_1, s_2] \propto \exp\left(-\frac{3}{2Na^2} \int_{s_1}^{s_2} \mathrm{d}s \left| \frac{\mathrm{d}}{\mathrm{d}s} \boldsymbol{r}_\alpha(s) \right|^2 \right). \quad (3)$$

Let us note that a is the segment size, and Na^2 is the mean squared end-to-end distance of a Gaussian chain. By the Kac–Feynman theorem, Eq. (2) can be related to a Fokker–Planck partial differential equation [2], known

also as modified diffusion equation (MDE) and shown with appropriate details below (Eqs. (16) and (17)).

Segments A and B interact via the χ parameter which provides an effective measure of incompatibility between them [1]. Evaluation of the full partition function of n interacting diblock chains, shown below (Eq. (4)), is a highly challenging task, involving many-body interactions, both intermolecular and intramolecular,

$$Z = \int \prod_{\alpha=1}^{n} \tilde{\mathcal{D}}\boldsymbol{r}_\alpha \delta\Big(1 - \hat{\phi}_A - \hat{\phi}_B\Big) \exp\Big(-\chi\rho_0 \hat{\phi}_A \hat{\phi}_B\Big), \tag{4}$$

where δ-function enforces incompressibility (the melt is assumed to be incompressible), and

$$\hat{\phi}_A(\boldsymbol{r}) = \frac{N}{\rho_0} \sum_{\alpha=1}^{n} \int_0^f \mathrm{d}s \delta(\boldsymbol{r} - \boldsymbol{r}_\alpha(s)), \tag{5}$$

$$\hat{\phi}_B(\boldsymbol{r}) = \frac{N}{\rho_0} \sum_{\alpha=1}^{n} \int_f^1 \mathrm{d}s \delta(\boldsymbol{r} - \boldsymbol{r}_\alpha(s)) \tag{6}$$

are the microscopic segments densities of A and B, respectively; $\rho_0 = nN/V$ is the segment number density. After replacing microscopic segment (or particle) densities with a variety of fields [2, 7–9], by inserting and spectrally decomposing the appropriate δ-functionals, the partition function of an incompressible diblock melt is

$$Z = \mathcal{N} \int \mathcal{D}\phi_A(\cdot)\mathcal{D}W_A(\cdot)\mathcal{D}\phi_B(\cdot)\mathcal{D}W_B(\cdot)\mathcal{D}\Psi(\cdot) \times \exp\left(-\frac{F[\phi_A, W_A, \phi_B, W_B, \Psi]}{k_\mathrm{B}T}\right), \tag{7}$$

where $\mathcal{N}$ is a normalization factor. The functional integral is taken over the relevant fields $\phi_A(\boldsymbol{r})$, $W_A(\boldsymbol{r})$, $\phi_B(\boldsymbol{r})$, $W_B(\boldsymbol{r})$, and $\Psi(\boldsymbol{r})$, with the free energy functional, $F[\phi_A, W_A, \phi_B, W_B, \Psi]$, including the single chain partition function (in external fields $W_A(\boldsymbol{r})$ and $W_B(\boldsymbol{r})$), as shown below

$$\frac{F[\phi_A, W_A, \phi_B, W_B, \Psi]}{nk_\mathrm{B}T} \equiv -\ln\frac{\mathcal{Q}}{V} + V^{-1}\int \mathrm{d}\boldsymbol{r}\Big[N\chi\phi_A(\boldsymbol{r})\phi_B(\boldsymbol{r}) - W_A(\boldsymbol{r})\phi_A(\boldsymbol{r}) - W_B(\boldsymbol{r})\phi_B(\boldsymbol{r}) - \Psi(\boldsymbol{r})(1 - \phi_A(\boldsymbol{r}) - \phi_B(\boldsymbol{r}))\Big]. \tag{8}$$

Fields $\phi_A(\boldsymbol{r})$ and $\phi_B(\boldsymbol{r})$ are associated with normalized concentration profiles of A and B, and fields $W_A(\boldsymbol{r})$ and $W_B(\boldsymbol{r})$ with chemical potential fields acting on A and B, respectively; field $\Psi(\boldsymbol{r})$ enforces incompressibility. Evaluating functional integrals in Eq. (7) is a challenging task which, in principle, can be performed by field theoretic simulations as proposed and implemented by Fredrickson and co-workers [2, 12]. A simpler, but approximate, approach is based on the mean-field idea, where the dominant, and in fact only, contribution to the functional integral in Eq. (7) comes from the fields satisfying the saddle point condition expressed as the following set of equations:

$$\frac{\delta F}{\delta\phi_A} = \frac{\delta F}{\delta\phi_B} = \frac{\delta F}{\delta W_A} = \frac{\delta F}{\delta W_B} = \frac{\delta F}{\delta\Psi} = 0. \tag{9}$$

Performing the above functional derivatives yields

$$W_A(\boldsymbol{r}) = N\chi\phi_B(\boldsymbol{r}) + \Psi(\boldsymbol{r}), \tag{10}$$

$$W_B(\boldsymbol{r}) = N\chi\phi_A(\boldsymbol{r}) + \Psi(\boldsymbol{r}), \tag{11}$$

$$1 = \phi_A(\boldsymbol{r}) + \phi_B(\boldsymbol{r}), \tag{12}$$

$$\phi_A(\boldsymbol{r}) = \frac{V}{\mathcal{Q}}\int_0^f \mathrm{d}s q(\boldsymbol{r}, s)q^\dagger(\boldsymbol{r}, s), \tag{13}$$

$$\phi_B(\boldsymbol{r}) = \frac{V}{\mathcal{Q}}\int_f^1 \mathrm{d}s q(\boldsymbol{r}, s)q^\dagger(\boldsymbol{r}, s), \tag{14}$$

where $\mathcal{Q}/V$ can be calculated as

$$\frac{\mathcal{Q}}{V} = \frac{1}{V}\int \mathrm{d}\boldsymbol{r} q(\boldsymbol{r}, 1) \tag{15}$$

and $q(\boldsymbol{r}, s)$ is the forward chain propagator which is the solution of the following modified diffusion equation:

$$\frac{\partial q}{\partial s} = \frac{1}{6}Na^2\nabla^2 q - W_A(\boldsymbol{r})q, \quad 0 \le s \le f,$$

$$\frac{\partial q}{\partial s} = \frac{1}{6}Na^2\nabla^2 q - W_B(\boldsymbol{r})q, \quad f \le s \le 1 \tag{16}$$

with the initial condition $q(\boldsymbol{r}, 0) = 1$. Similarly $q^\dagger(\boldsymbol{r}, s)$ is the backward chain propagator which is the solution of the conjugate modified diffusion equation

$$-\frac{\partial q^\dagger}{\partial s} = \frac{1}{6}Na^2\nabla^2 q^\dagger - W_A(\boldsymbol{r})q^\dagger, \quad 0 \le s \le f,$$

$$-\frac{\partial q^\dagger}{\partial s} = \frac{1}{6}Na^2\nabla^2 q^\dagger - W_B(\boldsymbol{r})q^\dagger, \quad f \le s \le 1 \tag{17}$$

with the initial condition $q^\dagger(\boldsymbol{r}, 1) = 1$.

While the set of Eqs. (10)–(14) can be solved, in principle, in a self-consistent manner, it is difficult to solve it without some additional assumptions. First, we assume that the melt forms a spatially ordered nanophase. Second, we use the UCA which is a considerable simplification, limiting our attention to a single D-dimensional spherical cell of radius R, and volume V. All fields, within this cell, have radial symmetry, which reduces this problem computationally to a single radial coordinate, r. The unconstrained spatial variables, specified in Table I for each d, become computationally irrelevant. Thus Eq. (15) can be rewritten as

$$\frac{\mathcal{Q}}{V} = D\frac{\int_0^R r^{D-1}q(r, 1)\,\mathrm{d}r}{R^D}. \tag{18}$$

Let us note that the factor, D, in front of the above integral originates from the ratio of the area of a sphere with radius 1 to the volume of a spherical cell with the same radius, both in D dimensions.

While in integrals (Eqs. (13)–(15)) we replace $\boldsymbol{r}$ with r, and $\mathrm{d}\boldsymbol{r}/V$ with $Dr^{D-1}\mathrm{d}r/R^D$, in the modified diffusion Eqs. (16) and (17), we replace $\boldsymbol{r}$ with r and use the spherically symmetric form of the Laplacian

$$\nabla^2 f = \frac{\partial^2 f}{\partial r^2} + \frac{D-1}{r}\frac{\partial f}{\partial r} \tag{19}$$

and similarly, in equations for both propagators $q(r,s)$ and $q^\dagger(r,s)$, we replace $\boldsymbol{r}$ with r. Obviously the solution depends on radius, R, and dimensionality, $D = 1, 2, 3$ and 4, corresponding to 4 different nanophases, shown in Table I. We use the Crank–Nicholson scheme (Appendix A) to solve iteratively the modified diffusion equations (Eqs. (16) and (17)) in their radial form, until the self-consistency condition is met, obtaining the saddle point fields, $\overline{\phi_A}(r)$, $\overline{\phi_B}(r)$, $\overline{W_A}(r)$ and $\overline{W_B}(r)$ for a given R and D. In the MF approximation, the free energy functional becomes the free energy, and therefore we calculate the reduced free energy (per chain in $k_\mathrm{B}T$ units) by substituting the saddle point fields into Eq. (8):

$$\frac{F(R,D)}{nk_\mathrm{B}T} \equiv -\ln\frac{\mathcal{Q}}{V} + \frac{D}{R^D}\int_0^R r^{D-1}\big[N\chi\overline{\phi_A}(r)\overline{\phi_B}(r) - \overline{W_A}(r)\overline{\phi_A}(r) - \overline{W_B}(r)\overline{\phi_B}(r)\big]\,\mathrm{d}r. \tag{20}$$

3. Results and discussion

Since in the MF theory, the stability of a nanophase depends on the product χN and composition, f, we start, at a given point of the phase diagram (χN, f), with numerical calculation of $F(R,D)$ (Eq. (20)) for numerous D's (1, 2, 3, and 4) and R's. In order to solve the MDE's (Eqs. (16) and (17)) we use up to $N_T = 160$ and up to $N_R = 800$ steps for the "time", s, and space, r, variables, respectively. Usually we need about 10^1 iterations (at selected points up to 10^3) to meet the self-consistency criteria with relative accuracy up to 10^{-6}. However, for selected points in the (χN, f)-plane, we increase both the number of steps and the desired accuracy of convergence.

Numerically, we find R and D which minimize $F(R,D)$, and this allows us to determine the dimensionality, D, of the most stable nanophase, and therefore the most favorable nanophase itself, using the correspondence from Table I. But the free energy of this nanophase has to be compared to that of the disordered phase. Therefore, we calculate the difference

$$\frac{\Delta F}{nk_\mathrm{B}T} \equiv \frac{F}{nk_\mathrm{B}T} - \frac{F_\mathrm{dis}}{nk_\mathrm{B}T}, \tag{21}$$

where F_dis is the free energy of the disordered phase

$$\frac{F_\mathrm{dis}}{nk_\mathrm{B}T} = N\chi f(1-f). \tag{22}$$

If ΔF is negative, then the appropriate nanophase is thermodynamically stable for the point considered, (χN, f); otherwise the system is the disordered phase.

This procedure allows us to map the DBC melt phase diagram for $4d$ in ($\chi N, f$)-plane, as shown in Fig. 1. Since there is a mirror symmetry with respect to $f = 0.5$ ($f \to 1-f$, A can be exchanged with B), we show the resultant nanophases only from $f = 0.5$ to 1, and the following phase sequence is observed: L, C, S_3, S_4, and the disordered phase. Solid lines between nanophases indicate the OOT lines, and a solid line between S_4 phase and disordered phase is the ODT (binodal) line; the corresponding data for those lines is presented in Table II (note that due to the mirror symmetry, f's are taken from 0 to 0.5). A new nanophase, S_4, is observed in a relatively narrow strip between the S_3 phase and disordered phase, which is the main difference between the $4d$ and $3d$ DBC phase diagrams. We extrapolate the calculated OOT lines, $f_{L/C}$, f_{C/S_3}, f_{S_3/S_4}, to the strong segregation limit, that is we estimate them as $\chi N \to \infty$ (or $1/(\chi N) \to 0$), fitting to the following function:

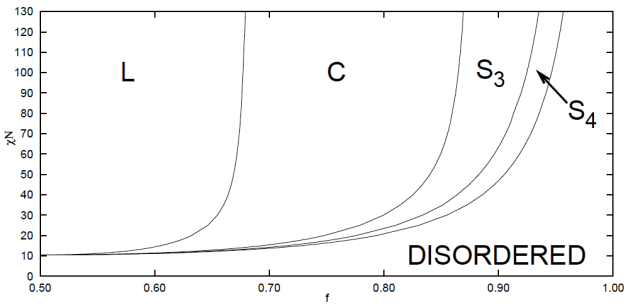

Fig. 1. DBC phase diagram in $4d$: L, C, S_3, and S_4 indicates corresponding nanophases; the disordered phase is also shown.

$$f(\chi N) = f^0 + \frac{g^0}{\chi N} \tag{23}$$

as used in Ref. [10], and to

$$f(\chi N) = f^1 + \frac{g^1}{(\chi N)^{1/3}} \tag{24}$$

as used in Ref. [33]. Unfortunately, we cannot find the limits, f^1, for f_{C/S_3} and f_{S_3/S_4} with the function from Eq. (24), because they depend significantly on the points selected for fitting. By contrast, the function from Eq. (23) gives consistent limits, f^0 (up to, at least, 2 significant figures), which do not depend strongly on the selection of points for $\chi N \geq 70$. The resultant limits, $f^0_{L/C}$, f^0_{C/S_3}, $f^0_{S_3/S_4}$ are compared to the SST f's, as shown in Table III. The relevant results of the SST calculations for an arbitrary D are shown in Appendix B. The discrepancy between the SST and the present SCFT with the UCA, for $f_{L/C}$ and f_{C/S_3} is within 2% error, as also reported in [10]. However, this discrepancy for f_{S_3/S_4} is about 10%. It seems that in order to increase the accuracy of the extrapolations, one should perform the SCFT calculations for higher χN's, but this may require a $4d$ extension of the method developed by Matsen [11, 16] and the SST with corrections. We also compare $f_{L/C}$ and f_{C/S_3} with the full SCFT (as presented in Ref. [10]), that is without using the UCA, and the overall agreement is again within 2% error.

While spinodals for the ODT calculated with random-phase approximation (RPA) [6] are the same for $d = 2$, 3, and 4, the binodals (the ODT lines), calculated in this work, depend on d as shown in Fig. 2. The binodals

TABLE II

The ODT and OOT lines for selected χN's.

χN	$f_{L/C}$	f_{C/S_3}	f_{S_3/S_4}	f_{ODT}
20	0.36797	0.25210	0.22436	0.20661
30	0.34531	0.20048	0.16643	0.14529
40	0.33601	0.17474	0.13631	0.11424
50	0.33120	0.15988	0.11714	0.09484
60	0.32828	0.15059	0.10379	0.08166
70	0.32629	0.14452	0.09387	0.07188
80	0.32482	0.14057	0.08698	0.06455
90	0.32392	0.13737	0.08029	0.05854
100	0.32303	0.13510	0.07535	0.05376
110	0.32242	0.13334	0.07125	0.04977
120	0.32152	0.13190	0.06780	0.04638
130	0.32090	0.13070	0.06486	0.04344

TABLE III

The OOT lines from the full SCFT [10] and UCA extrapolated to infinite χN's compared to the SST results.

Method	$f_{L/C}$	f_{C/S_3}	f_{S_3/S_4}
full SCFT [10]	0.3100	0.1050	–
UCA	0.3150	0.1149	0.0306
SST	0.2845	0.1172	0.0336

depend weakly on d, and they are particularly close to each other in the vicinity of $f_A = 1/2$ (symmetric diblock), and therefore we show them in a narrow window (from 0.9 to 0.95 in f, that is away from $f = 1/2$) in the inset of Fig. 2. We observe the following sequence of binodals: the upper line corresponds to the $2d$ binodal, the medium one to the $3d$, and the lower to the $4d$ binodal. For $f = 1/2$ the RPA spinodal is at $(\chi N)_{\mathrm{c}} \approx 10.4949$, and the calculated binodals (for $d = 2$, 3, and 4) also converge to this point within the numerical accuracy. Similarly, the OOT lines seem to converge to $(\chi N)_{\mathrm{c}}$ for $f = 0.5$.

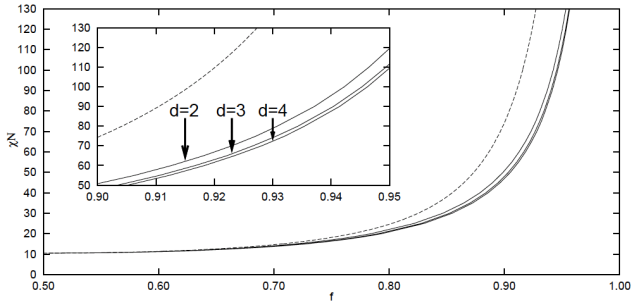

Fig. 2. Binodals are indicated by solid lines: upper — $2d$, middle — $3d$, and lower — $4d$; the RPA spinodal by the dotted line. nset shows the phase diagram from $f = 0.90$ to 0.95.

Finally, we consider the potential relevance of the $4d$ results. While the sequence of phases (layers, cylinders, $3D$ spherical cells, and $4D$ spherical cells) is not unexpected, the (χN)-dependent width of the stability window for the S_4 case cannot be easily estimated without performing the SCFT calculations. It is reassuring to find that the SST of zeroth order recovers the SCFT limits for $d = 4$ as it does for $d = 2$ and 3. Also the weak d-dependence of the binodals is of potential interest. It is still premature to justify the practical advantages of this study, but it sheds some light on the underlying theory of block copolymer melts.

4. Conclusions

Using a self-consistent field theory in spherical unit cells of various dimensionalities, $D = 1$, 2, 3, and 4, we calculate phase diagram of a diblock, A-b-B, copolymer melt in 4 dimensional space, $d = 4$. The phase diagram is parameterized by the chain composition, f, and incompatibility between A and B, quantified by the product χN. We predict 4 stable nanophases: layers, cylinders, $3D$ spherical cells, and $4D$ spherical cells, and calculate both order–disorder and order–order transition lines. In the strong segregation limit, that is for large χN, the OOT compositions, $f_{L/C}$, f_{C/S_3}, and f_{S_3/S_4} are determined by the strong segregation theory. Those transitions are close to the corresponding extrapolations from the self-consistent field theory, as shown in Table III. We find that the S_4 nanophase is stable in a narrow strip between ordered S_3 nanophase and the disordered phase. The calculated binodals (ODT lines) depend weakly on d. Finally, the SST of zeroth order works reasonably well as the limiting case of the SCFT for different dimensionalities, including $D = 4$, but the fitting procedure is open to debate, since the role of higher order corrections in the SST seems to be unexplained.

In summary we find answers to some questions that we pose in Introduction:

1. the nanophase S_4 is stable within a relatively narrow strip between the S_3 nanophase and the disordered phase,
2. the sequence of nanophases appropriate for the UCA in $3d$ is preserved, starting from $f = 1/2$, L, C, S_3, and there is an additional S_4 nanophase in $4d$,
3. the ODT binodals depend weakly on d, and they are shifted as d is varied,
4. the SST compositions, $f_{L/C}$, f_{C/S_3}, and f_{S_3/S_4} are close to the corresponding extrapolations from the self-consistent field theory, as shown in Table III, but the fitting procedure is open to debate.

Finally, the questions concerning the fluctuation--enhanced formation of the non-classical nanophases, for higher d's, remains open. To address this question an inclusion of fluctuations is required via, for example, field theoretic simulations [2] and also allowing non-spherical symmetries of the nanophase, but this is beyond the scope of this study.

Acknowledgments

Grant N204 125039 of the Polish Ministry of Science and Higher Education is gratefully acknowledged. We also acknowledge a computational grant from the Poznań Supercomputing and Networking Center (PCSS). M.B. thanks M.D. Whitmore and J.D. Vavasour for fruitful discussions, and also gratefully acknowledges significant comments from M.W. Matsen, concerning extrapolations in the strong segregation limit.

Appendix A

The Crank–Nicholson method of solving the modified diffusion equation (MDE) is briefly sketched below. Numerically, we discretize $q(r,s)$:

$$q_i^n = q(i\Delta r, n\Delta s), \quad w_i = W_A(i\Delta r), \tag{25}$$

where $i = 1, 2, \ldots, N_R$, and $n = 1, 2, \ldots, N_T$. Using numerical form of derivatives we can write the MDE (this is for the forward propagator from 0 to f, but other propagators can be written similarly) as

$$\begin{aligned}
\frac{q_i^{n+1} - q_i^n}{\Delta s} &= \frac{1}{2}\frac{Na^2}{6}\frac{q_{i+1}^n + q_{i-1}^n - 2q_i^n}{(\Delta r)^2} \\
&+ \frac{1}{2}\left(\frac{Na^2}{6}\frac{D-1}{i\Delta r}\frac{q_{i+1}^n - q_{i-1}^n}{2\Delta r} - w_i q_i^n\right) \\
&+ \frac{1}{2}\frac{Na^2}{6}\frac{q_{i+1}^{n+1} + q_{i-1}^{n+1} - 2q_i^{n+1}}{(\Delta r)^2} \\
&+ \frac{1}{2}\left(\frac{Na^2}{6}\frac{D-1}{i\Delta r}\frac{q_{i+1}^{n+1} - q_{i-1}^{n+1}}{2\Delta r} - w_i q_i^{n+1}\right),
\end{aligned}$$

which can be rewritten in a trigonal matrix form

$$\begin{bmatrix} b_1 & a_1 & 0 & 0 & \ldots & 0 \\ c_2 & b_2 & a_2 & 0 & \ldots & 0 \\ \ldots & & & & & \ldots \\ 0 & 0 & 0 & \ldots & c_{N_R} & b_{N_R} \end{bmatrix} \begin{bmatrix} q_1^{n+1} \\ q_2^{n+1} \\ \ldots \\ q_{N_R}^{n+1} \end{bmatrix} = \begin{bmatrix} d_1 \\ d_2 \\ \ldots \\ d_{N_R} \end{bmatrix}, \tag{26}$$

where

$$a_i = \frac{1}{2}A\left(1 + \frac{D-1}{2i}\right), \quad c_i = \frac{1}{2}A\left(1 - \frac{D-1}{2i}\right),$$

$$b_i = -1 - A + \frac{1}{2}w_i\Delta s, \tag{27}$$

$$d_i = -\frac{1}{2}\left[A(q_{i+1}^n + q_{i-1}^n - 2q_i^n) + A\frac{D-1}{2i}(q_{i+1}^n - q_{i-1}^n) + w_i q_i^n \Delta s\right] - q_i^n, \tag{28}$$

$$A = \frac{Na^2\Delta s}{6(\Delta r)^2}. \tag{29}$$

Equation (26) can be effectively solved (for $\boldsymbol{q}^{n+1}$) by upper-lower decomposition of the trigonal matrix [2, 34].

Appendix B

The SST for diblock melts was developed by Semenov [32], and later modified by Likhtman and Semenov [33] to include corrections, but we use it without corrections (zeroth order), as presented by Matsen in Refs. [17, 35], with the following expression for the free energy per chain:

$$\frac{F_{\mathrm{SST}}}{kTn} = \alpha^A\frac{R^2}{Na^2} + \alpha^B\frac{R^2}{Na^2} + \beta(\chi N)^{\frac{1}{2}}\left(\frac{R}{aN^{\frac{1}{2}}}\right)^{-1}, \tag{30}$$

where the first term is the stretching energy of the A-block, the second term is the stretching energy of the B-block, the third term is the interfacial energy in strong segregation. The A-segments are distributed in the spherical core of radius $R_I = f^{1/D}R$, the interface is sharply localized at $r = R_I$, and the B-segments can be found in the spherical layer from $r = R_I$ to R. We calculate the coefficients, α^A, α^B, and β, for an arbitrary dimensionality, D, by a straightforward generalization of the approach presented in [35]:

$$\alpha^A = \frac{3\pi^2 f^{(2-D)/D}}{4(D^2+3D+2)}, \tag{31}$$

$$\alpha^B = \frac{3\pi^2\left[D^2\left(f^{1/D}-1\right)^2 - 2(f-1)f^{2/D} + D\left(3f^{2/D} - 4f^{1/D} + 1\right)\right]}{8(D^2+3D+2)(f-1)^2}, \tag{32}$$

$$\beta = [Df^{(\mathrm{D}-1)/\mathrm{D}}]/\sqrt{6}. \tag{33}$$

Those coefficients reduce to expressions presented in Ref. [35] for L, C, and S_3, corresponding to $D = 1$, 2, and 3, respectively. By minimizing Eq. (30) with respect to R we obtain the equilibrium R which depends both on f and D:

$$R = a\left\{\beta/[2(\alpha^A + \alpha^B)]\right\}^{1/3}\chi^{1/6}N^{2/3} \tag{34}$$

and the minimum free energy is

$$\frac{F_{\mathrm{SST}}}{kTn} = \frac{3}{2}\left[2\left(\alpha^A + \alpha^B\right)\beta^2\chi N\right]^{1/3}. \tag{35}$$

The phase boundaries can be calculated as

$$f_{L/C} = (8 + 4\sqrt{2})/48 \approx 0.284517, \tag{36}$$

$$f_{C/S_3} \approx 0.117192, \tag{37}$$

$$f_{S_3/S_4} \approx 0.0335796, \tag{38}$$

and additionally (detailed calculations for $d = 5$ we present in Ref. [36])

$$f_{S_4/S_5} \approx 0.000183905. \tag{39}$$

The numerical values in Eqs. (38) and (39), and coeffi-

cients α^A, α^B, and β for an arbitrary D (Eqs. (31)–(33)), are reported, to our knowledge, for the first time. It is worth to notice that the phase boundaries, $f_{L/C}$, f_{C/S_3}, and f_{S_3/S_4}, do not depend on numerical prefactors such as $3\pi/8$ (in Eqs. (31) and (32)) and $1/\sqrt{6}$ (in Eq. (33)).

References

[1] P.G. de Gennes, *Scaling Concepts in Polymer Physics*, Cornell University Press, Ithaca 1979.

[2] G.H. Fredrickson, *The Equlibrium Theory of Inhomogeneous Polymers*, Clarendon Press, Oxford 2006.

[3] I.W. Hamley, *Developments in Block Copolymer Science and Technology*, Wiley, Berlin 2004.

[4] T.S. Bailey, C.M. Hardy, T.H. Epps, F.S. Bates, *Macromolecules* **35**, 7007 (2002).

[5] M. Takenaka, T. Wakada, S. Akasaka, S. Nishisuji, K. Saijo, H. Shimizu, M.I. Kim, H. Hasegawa, *Macromolecules* **40**, 4399 (2007).

[6] L. Leibler, *Macromolecules* **13**, 1602 (1980).

[7] M. Banaszak, M.D. Whitmore, *Macromolecules* **25**, 3406 (1992).

[8] J.D. Vavasour, M.D. Whitmore, *Macromolecules* **25**, 5477 (1992).

[9] M.W. Matsen, M. Schick, *Phys. Rev. Lett.* **72**, 2660 (1994).

[10] M.W. Matsen, M.D. Whitmore, *J. Chem. Phys.* **105**, 9698 (1996).

[11] M.W. Matsen, *J. Chem. Phys.* **114**, 10528 (2001).

[12] E.M. Lennon, K. Katsov, G.H. Fredrickson, *Phys. Rev. Lett.* **101**, 138302 (2008).

[13] T. Taniguchi, *J. Phys. Soc. Jpn.* **78**, 041009 (2009).

[14] I.W. Hamley, *Prog. Polym. Sci.* **34**, 1161 (2009).

[15] E.W. Cochran, C.J. Garcia-Cervera, G.H. Fredrickson, *Macromolecules* **39**, 2449 (2006).

[16] M.W. Matsen, *Europ. Phys. J. E* **30**, 361 (2009).

[17] M.W. Matsen, in: *Soft Condensed Matter*, Vol. 1, Eds. G. Gompper, M. Schick, Wiley, Berlin 2005.

[18] E.W. Cochran, C.J. Garcia-Cervera, G.H. Fredrickson, *Macromolecules* **39**, 2449 (2006).

[19] A.K. Khandpur, S. Forster, F.S. Bates, I.W. Hamley, A.J. Ryan, W. Bras, K. Almdal, K. Mortensen, *Macromolecules* **28**, 8796 (1995).

[20] X. Cheng, L. Lin, W. E, P. Zhang, A.-C. Shi, *Phys. Rev. Lett.* **104**, 148301 (2010).

[21] W. Li, W. Jiang, *Polym. Bull.* **64**, 805 (2010).

[22] T. Suo, D. Yan, S. Yang, A.-C. Shi, *Macromolecules* **42**, 6791 (2009).

[23] W. Song, P. Tang, H. Zhang, Y. Yang, A.-C. Shi, *Macromolecules* **42**, 6300 (2009).

[24] Y.A. Kriksin, P.G. Khalatur, I.Y. Erukhimovich, G. Ten Brinke, A.R. Khokhlov, *Soft Matter* **5**, 2896 (2009).

[25] Y. Zhuang, J. Lin, L. Wang, L. Zhang, *J. Phys. Chem. B* **113**, 1906 (2009).

[26] G.H. Fredrickson, E. Helfand, *J. Chem. Phys.* **87**, 697 (1987).

[27] S.A. Brazovskii, *Sov. Phys. JETP* **41**, 85 (1975).

[28] M.W. Matsen, G.H. Griffiths, R.A. Wickham, O.N. Vassiliev, *J. Chem. Phys.* **124**, 024904 (2006).

[29] S. Woloszczuk, M. Banaszak, P. Knychala, M. Radosz, *Macromolecules* **41**, 5945 (2008).

[30] M.W. Matsen, *J. Phys., Condens. Matter* **14**, R21 (2002).

[31] M.W. Matsen, *Europ. Phys. J. E* **33**, 297 (2010).

[32] A.N. Semenov, *Sov. Phys. JETP* **61**, 733 (1985).

[33] A.E. Likhtman, A.N. Semenov, *Europhys. Lett.* **51**, 307 (2000).

[34] W.H. Press, B.P. Flannery, S.A. Teukolsky, W.T. Vetterling, *Numerical Recipes. The Art of Scientific Computing*, Cambridge University Press, Cambridge 1989.

[35] M.W. Matsen, F.S. Bates, *J. Chem. Phys.* **106**, 2436 (1996).

[36] M. Dziecielski, K. Lewandowski, M. Banaszak, *Computat. Methods Sci. Technol.* **17**, 17 (2011).